Journal of Civil Engineering and Architecture 19 (2025) 66-73
doi: 10.17265/1934-7359/2025.02.002

Ultrasonic Motor Using First and Second Bending Modes

G. M'Boungui
Department of Electrical Engineering, Tshwane University of Technology, Pretoria 0001, South Africa

Abstract: This paper presents the design of a novel resonator for use in a piezoelectric linear ultrasonic motor. the work is motivated by a motor previously developed by the authors that showed to be capable of achieving a force of 50 mn and a velocity of 14 mm/s, which they found unsatisfactory. to that end, among an existing variety of working principles for piezoelectric ultrasonic motors, the principle of giving the material points of the stator in contact with the rotor a "∞" trajectory and thus propelling the rotor was utilized. our concept is based on Euler-Bernoulli beam theory which shows that the natural frequency ratio of the first and second bending modes for a beam, fixed at both ends, is approximately 3 and we employ a gradient-based optimization algorithm to assist in the design of the structure.

Key words: Lissajous pattern, piezoelectric ultrasonic motor.

1. Introduction

Ultrasonic motors (USMs) have several advantages over conventional electromagnetic motors, and as a result these devices have attracted considerable attraction in recent years. The most significant advantages include their low speed and high torque characteristics, eliminating the need for gearing in certain applications; their amenability to miniaturisation; their relative simplicity in production; the fact that they do not cause nor are they affected by electromagnetic radiation and various others [1].

USMs appear in various sizes, shapes and forms (see [1] for an overview) but the general operating principle may be illustrated using the driving technique employed by the famous Sashida travelling wave rotary motor [2]. This motor uses a travelling wave generated by superimposing two standing waves with equal natural frequencies, but whose phases differ by 90° from each other in space and time. The result is that each contact point on the stator produces an elliptical locus of points in time. This requires the use of one electronic amplifier per mode.

Alternatively, the principle of giving the material points of the stator in contact with the rotor a Lissajous pattern trajectory and thus propelling the rotor was utilized by the authors [3]. Fleisher et al. [4] utilized the same principle earlier. The resonator has two natural modes with resonant frequencies in an integer ratio of 1:2. However, the authors found unsatisfactory the performance achieved by the obtained motor.

Our concept is based on Euler-Bernoulli beam theory which shows that the natural frequency ratio of the first and second bending modes for a beam, fixed at both ends, is approximately 1:3 and a gradient-based optimization algorithm is employed to assist in the design of the structure.

The working principle of the motor is first described. It consists of a rotor which is driven by the contact point as a result of its intermittent pressure against the resonator and a generated dry friction. Later the resonator is summarised, leading to a finite element mesh, used to analyse and manufacture the device. From there a vibrator free characterisation is conducted

Corresponding author: G. M'Boungui, research fields: electrical power engineering power systems analysis.

and a test performed to show the correct operation of the design.

2. Motor Design and Working Principle

USM employing the working principle developed by Sashida [2] exploit the propagation of a travelling wave in a resonator (stator) and the friction intermittently created while in contact with a slider or a rotor pressed against the resonator as shown in the figure 1 a) [2]. The superimposition of two standing waves with a phase difference of 90° both in space and time creates the travelling wave. In this case, the locus of the contact point is an ellipse that is exploited to drive the slider (or the rotor) and the use of two electronic amplifiers is required. An alternate scheme, which uses only one amplifier, was demonstrated by Flesher et al [4].

For the traditional operating principle of the Sashida motor [2], the trajectory of a contact point on the stator would form an ellipse as illustrated in Figure 2(a). On the other hand, in the scheme of Flesher et al [4] the resonator is designed to use two vibratory modes with the resonant frequency of the second mode being an integer multiple of the resonant frequency of the first mode. If the integer multiple is “3” then the figure-of-eight-plus pattern shown in figure 1 d) is produced.

In figure 1 d), if we assume that one mode contributes motion in the x direction and the second mode, in the y direction, then Equation (1) and (2) can be used to describe the trajectory of the contact point.

$$x = x_0 \sin(\omega t) \tag{1}$$

$$y = y_0 \sin(n\omega t + \varphi) \tag{2}$$

with ω the vibratory frequency in rad/s, φ, the phase difference between *x* and *y*, and *n* a real number. In particular, n=1, $\varphi = \frac{\pi}{2}$, was used to generate the ellipse, $n = \frac{1}{2}$, $\varphi = 0$ to generate the “∞” and $n = \frac{1}{3}$, $\varphi = 0$ to generate the “eight-plus” in figure 1 d).

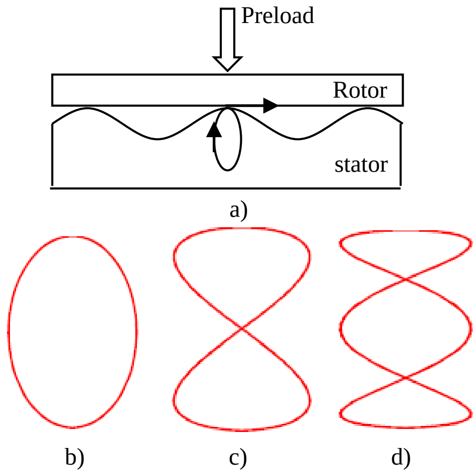

Fig. 1 USM principle and contact point trajectories a) driving principle for motor with elliptical trajectory b) output trajectories for case with n=1, φ=π/2, c) n=1/2, φ=0 or π and d) n=1/3, φ=0 or π.

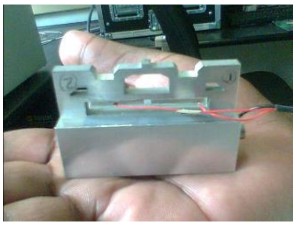

Fig. 2 Photograph of the resonator presented in [3].

The manual design of a resonator with two resonant frequencies an integer multiple of each other is a relatively challenging and iterative procedure. Recently, the authors employed topology optimization techniques to effectively automate the design of a resonator (figure 2) with a frequency ratio of two [3]. Although the design was successfully synthesised using the proposed method, the physical prototype resonator did not achieve vibratory amplitudes large enough to drive a slider with significant force. This is presumably due to the fact that the optimization formulation did not consider how strongly the ceramics drive the targeted resonant modes, but concentrated only on achieving the desired frequency ratio. This issue will be addressed in the current paper, based on a simplified beam-like resonator structure.

3. Resonator Design

USMs exploiting first bending – fourth longitudinal mode have been reported in literature (see for example

[5]). The USM proposed by Zhai et al. [5][6] was one of those. Its dimensions were 80 x 10.1 x 7.7 mm3 and it achieved a speed of 300 mm/s under 10 V and a loading capacity of 95 g. Similarly the design from Park et al. [5][7], was 65 mm x 5 mm x 18.3 mm and achieved a 600 mm/s speed and a 0.1 N force. The motors listed above are still rather large.

Bein et al. [8] developed a compact and simple ultrasonic motor using a beam-like resonator. Specifically, their resonator employed the first longitudinal and forth bending vibration modes of a free-free beam to achieve the required horizontal and vertical motions, respectively. However, their free-free beam configuration makes mounting the resonator without interfering with the targeted modes challenging.

Using Euler-Bernoulli beam theory, it can be shown that the natural frequency ratio of the first and second bending modes for a beam, fixed at both ends, is approximately 3 [9]. Although a more detailed finite element analysis is necessary to fine-tune the design and to capture important effects not considered in the simple beam model, this simple analytical model is used to suggest suitable starting resonator geometry, schematically depicted in Figure 4. This structure has a first bending mode producing vertical displacement, and the second bending mode producing a horizontal displacement at approximately three times the frequency of the vertical displacement, as introduced in Figure 3. The result is a contact point trajectory depicted in Figure 1 c), which can effectively be used to drive a slider or rotor. Furthermore, the fact that the proposed resonator is fixed on both ends alleviates many of the mounting problems of the resonator Bein et al. proposed [8]. It is to notice that the fixed-fixed beam boundary conditions mentioned above are simulated thanks to the relatively massive block which the subset piezoceramics-beam is attached to on figure 3.

3.1 Optimization Problem Formulation

A great deal of research has been carried out in the field of optimization of smart structures and actuators [10]. The primary potential of using optimization in structural engineering is probably to size the elements composing a structure [11]. The study deals with optimization of the size of the actuator assuming the passive structure is of predetermined geometry and material. Therefore almost all of the work is focused on optimal placement of piezoelectric ceramics on a beam. More precisely, maximizing the coupling factor to be discussed shortly is considered as the objective in the problem. The design variables are the geometric coordinates of the structure including the size and position of the ceramics. Constraint is imposed on the resonant frequency ratio of “3”.

3.2 Coupling Factor

The electromechanical coupling factor k is one of the important figures of merit in piezoelectric transducers [12]. The term electromechanical coupling factor relates to the ability of the transducer to convert electrical energy to mechanical energy or vice versa. The effective coupling factor may be written as:

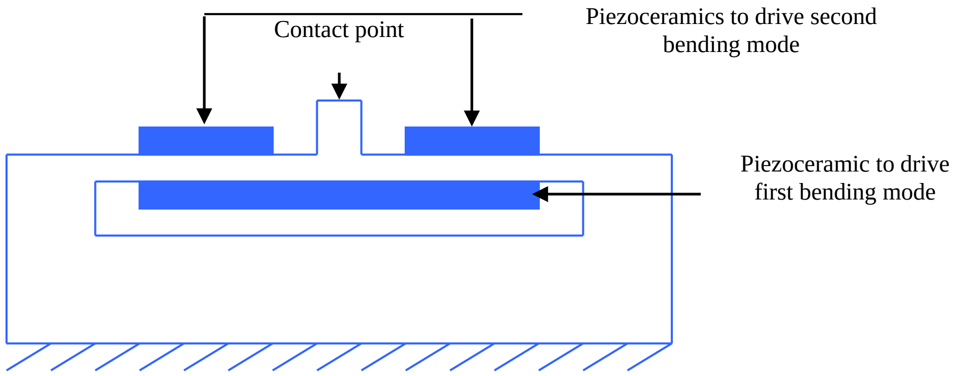

Fig. 3 Schematic of proposed resonator structure.

$$k_i^2 = \frac{\omega_{oci}^2 - \omega_{sci}^2}{\omega_{oci}^2} \qquad (3)$$
$$i = 1,2$$

with the angular resonance frequency (short circuit) ω_{sci} and angular antiresonance frequency (open circuit) ω_{oci}. The boundary conditions yield the characteristic equations for open and closed electrodes.

3.3 Problem Statement

The design goal is to simultaneously achieve the targeted natural frequency ratio between the first and second bending modes of 3, while strongly driving the two targeted modes. The optimization variables will describe the structural geometry (size and placement of piezoelectric ceramics, etc.). If the optimization variable $x= (x_1, x_2, \ldots, x_n)$ with $n = 13$, $j = 1,..,n$ and x_j the geometric coordinates introduced above, what appears a non-linear constrained problem becomes:

Find

$$\underline{x} = (x_1, x_2, \ldots, x_n)$$

To maximise

$$f(\underline{x}) = f(k_1, k_2) \qquad (4)$$

Subject to

$$\frac{eigen - frequency2}{eigen - frequency1} = 3$$

where eigen-frequency1 and eigen-frequency2 are respectively the first and the second natural frequency.

Matlab® computing environment is chosen to run the gradient-based algorithm available through built-in optimization toolbox. Therefore, the constrained optimization problem is adapted to form an unconstrained optimization problem using the penalty method. The problem can be restated:

$$\min_{\underline{x}} f(\underline{x}) \qquad (5)$$

$$f(\underline{x}) = -(\log_{10} k_1^2 + \log_{10} k_2^2) + p\left(\frac{eigen - frequency2}{eigen - frequency1} - 3\right)^2 \qquad (6)$$

That is about minimizing the function f that depends on optimization variable x. The penalty factor p was chosen equal to 10.

From a practical point of view a commercial available Finite Element Modelling package, namely Abaqus® that provides the ability to be linked to Matlab® is coupled to Matlab® so that the two software become one and program runs in Matlab®. Details to run optimization algorithms can be found in the *Optimization Toolbox™ 3 user's guide* (The *MathWorks™* 2007b) while details on writing an Abaqus Input file from Matlab®, that is text manipulation, are available in [13]. The resonator was modelled with 3D cubic elements with 8 nodes (C3D8 and C3D8E). As a result, the 3 Dimension model (block of 25.3 x 18.05 x 8.23 mm) which the detailed mesh is shown in figure 4 a) that also shows the two targeted eigen-modes was obtained

4. Resonator Vibration Characterisation

The first experimental investigation started on a prototype of the non-optimized resonator (25.9 x 18 x 7 mm) before it is part of assembled motor. For that purpose, the setup illustrated in figure 5 was realised. The setup consists on a Polytec Scanning Vibrometer PSV 4000 represented figure 5 a). The first part of the investigation aims to experimentally identify the targeted resonator vibratory modes. To that end, the output signal was generated from the internal generator (within the control unit) and linearly amplified using an AA LAB Systems LTD A-303 High Voltage Amplifier. That signal was used to drive the piezoceramics in the frequency range of 8-50 kHz. As a result, the first and second bending modes were respectively located at 13.281 and 40.701 kHz that is a ratio of 3.06 in agreement with the FEM prediction of 3.03.

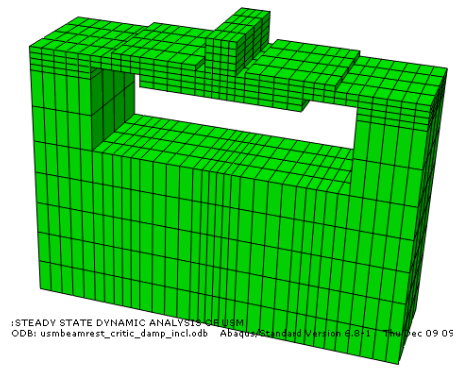

(a)

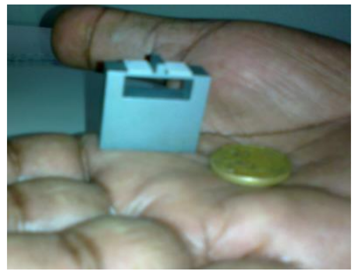

(b)

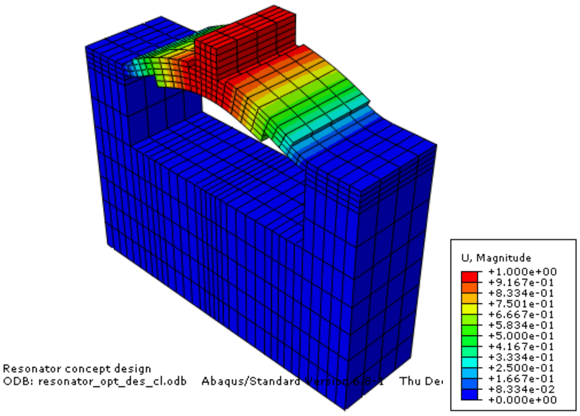

(c)

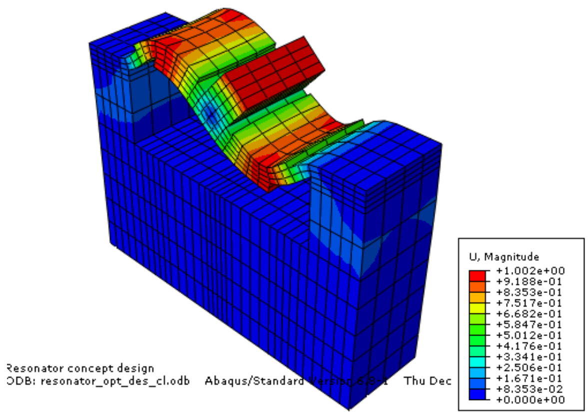

(d)

Fig. 3 a) Finite element result resonator mesh, b) photograph of the designed resonator, c) first and d) second bending modes producing vertical and horizontal displacements, respectively.

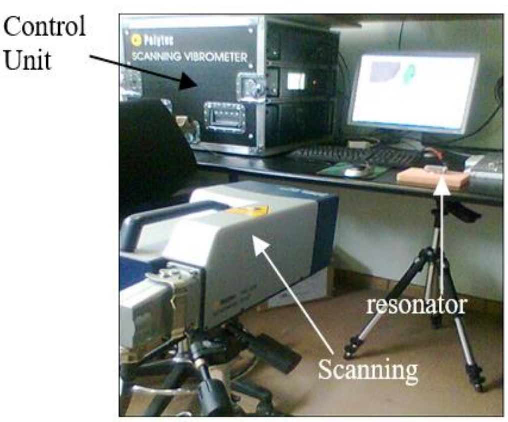

(a)

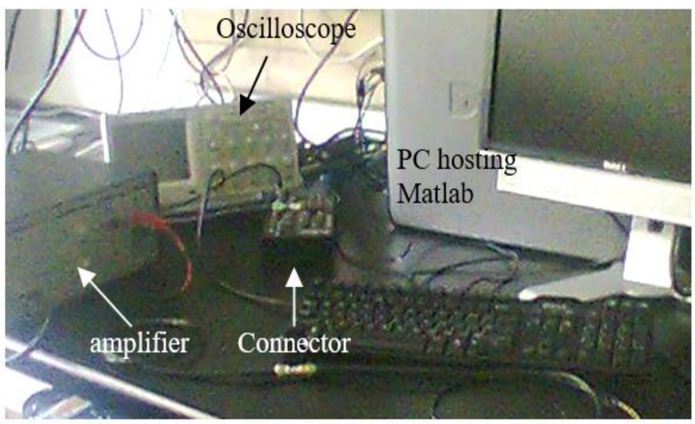

(b)

Fig. 5 Experimental setup a) Polytec Scanning Vibrometer PSV 4000, b) Matlab® signal generator.

The second part of our investigation deals with the plot of the locus of the stator output point; both the normal (to the base) and the in-plane displacements are required. In its usual configuration, the laser vibrometer measures only the normal displacements. In other words, the vibration measurement is available only in the direction of the optical axis. Therefore, the modified experimental setup depicted in figure 6 was required in order to obtain the displacements represented by vector v1 or v2 in figure 6.

Our driving signal containing the two targeted frequencies was generated using the Matlab Data Acquisition Toolbox (figure 5 b)). The velocity of the contact point v_1, was then measured with the device at $\theta = 30^0$ with respect to the beam as sketched in figure 6. The experiment was then repeated with $\theta = -30^0$ with resultant velocity v_2. A transformation equation (7) was used to determine the in-plane v_x and normal v_y velocities:

$$\begin{bmatrix} v_x \\ v_y \end{bmatrix} = \begin{bmatrix} \sin\theta & \cos\theta \\ -\sin\theta & \cos\theta \end{bmatrix}^{-1} \begin{bmatrix} v_1 \\ v_2 \end{bmatrix} \tag{7}$$

In the figures 7 a) and 7 b) the continuous-time variations of the excitation and measured signals $v_i(i=1,2)$ are presented. The computed in-plane and normal velocities v_x and v_y are plotted (figure 7 c) and 7 d)). Lastly the in-plane displacement is plotted vs. the normal displacement to yield the figure-of-eight-plus trajectory in the figure 7 e).

The investigation is finalized with a comparison between the displacements obtained from the resonator in figure 2 and the one analysed in this section 4. For that the two resonators were supplied approximately under the same conditions of peak-to-peak voltages and each one at its eigen-frequencies. That later investigation was justified by the fact that the higher the contact displacement more significant is the thrust to be developed by the motor. Shown in figure 8 a) is the voltage supply (oscilloscope channel 2, scale 5.0 V/division) that comprises two sine waves in a ratio of 1:2 while the voltage supply (oscilloscope channel 2, scale 5.0 V/division) in figure 8 b) consists of two sine waves in a ratio of 1:3. As a response to the two different excitations described above, the signals captured from the oscilloscope show a maximum displacement of 10 V equivalent to 0.5 μm for the later design (figure 8 b); channel 1, scale 5.0 V/division) and 3.26 V equivalent to 0.165 μm for the precedent design (figure 8 a); channel 1, scale 2.0 V/division).

To confirm that the resonator operated correctly, the piezoceramics were properly supplied with a signal containing 13.281 and 40.701 kHz and approximately 160 V peak. A ball bearing of 20 mm diameter mounted on a fixed shaft pressed against the output point of the resonator lying down in a sponge resulted in the rotation of the bearing ball in either direction accordingly with the phase difference φ introduced in section 2.

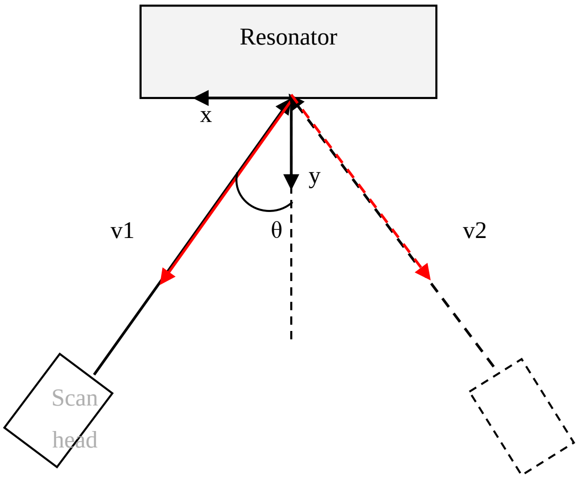

Fig. 4 Set-up to measure point normal and tangential velocity components.

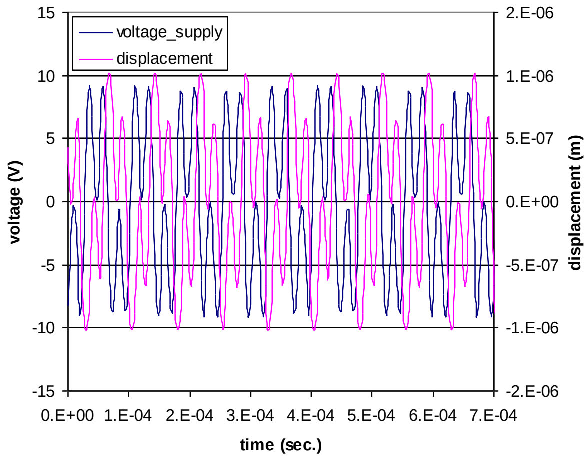

a) Measured signal *v1*

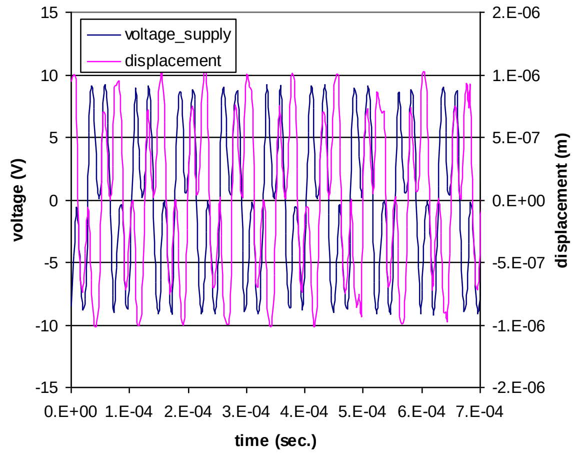

b) Measured signal *v2*

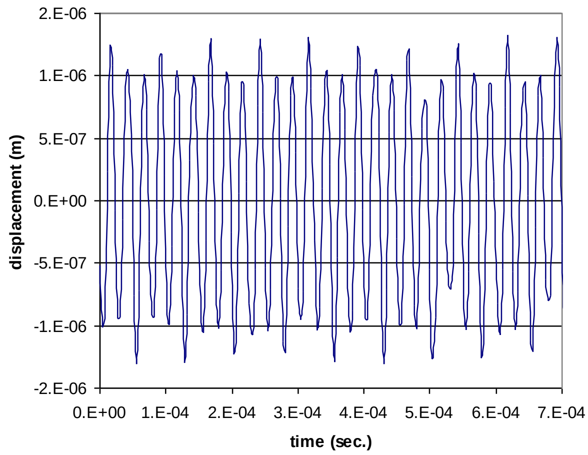

c) Computed signal *vx*

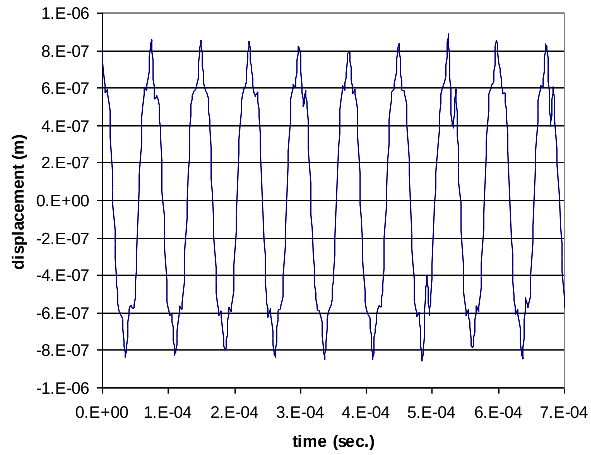

d) Computed signal *vy*

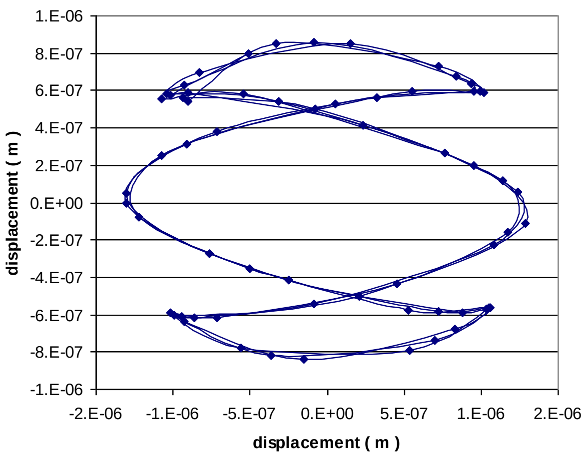

e) Computed output point trajectory

Fig. 7 Measured normal and tangential point velocity components and figure-of-eight output trajectory.

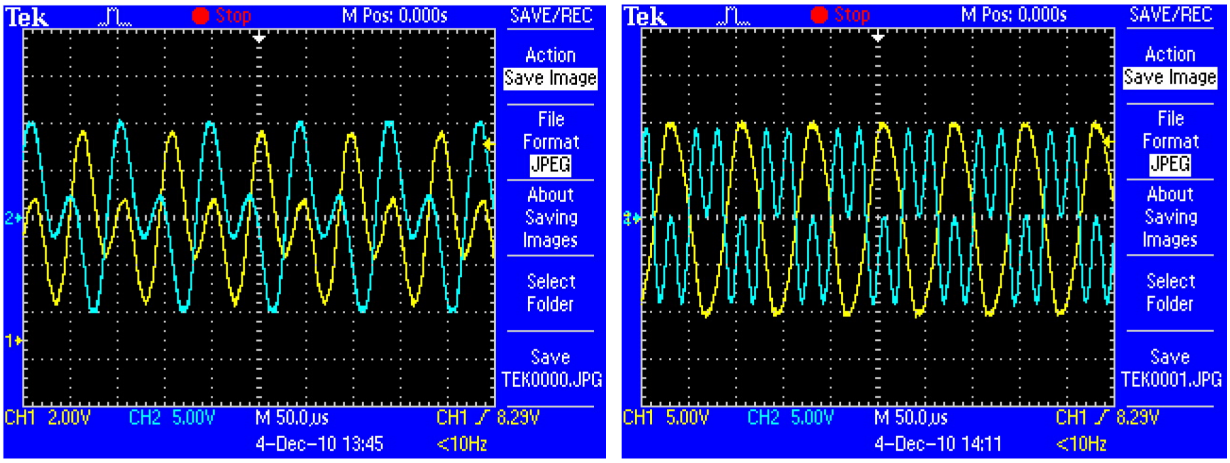

a) b)

Fig. 5 a) Signals related to resonator in [3] output point displacement; b) Signals related to current design output point displacement.

5. Conclusion

The proposal is a beam-like structure exploiting first and second bending modes whose corresponding resonant frequencies have a ratio of 1:3. The coupling factor was chosen as figure of merit to optimize the current resonator using optimisation algorithm available through Matlab® optimization toolbox.

A non-optimized resonator prototype already shows a greater targeted contact point maximum displacement with respect to the previous design. Yet the two coupling factors of the prototype are lower compared to the ones obtained with the optimized structure. A greater displacement and therefore thrust to be developed by the compact device described in this paper is a fortiori expected.

References

[1] K. Uchino, Piezoelectric ultrasonic motors: overview**,** *Smart Mater. Struct*. **7**, 273–285, Printed in the UK, 1998.

[2] T. Sashida, T. Kenjo, *Introduction to ultrasonic motors*, Oxford Univ. Press, New York (United States) 01 Jan 1993.

[3] G. M'Boungui, P.W. Loveday and C.S. Long, Experimental Development of an Ultrasonic Linear Motor, Seventh South African Conference on Computational and Applied Mechanics SACAM, Pretoria, 10-13 January 2010.

[4] M. Fleischer, D. Stein and H. Meixner, New Type of Piezoelectric Ultrasonic Motor, *IEEE Transactions on ultrasonics, ferroelectrics, and frequency control*, vol. 36, No. 6, November 1989.

[5] S. Dembélé, K. Rochdi, A 3 DOF linear ultrasonic motor for transport and micropositioning, *Sensors and Actuators A Physical* 125, 486-493, 2006.

[6] B. Zhai, S-P. Lim, K-H. Lee, S. Dong and P. Lu, A modified ultrasonic linear motor, *Sensors and Actuators*, 86: 154–158, 2000.

[7] T. Park, B. Kim, M-H. Kim and K. Uchino, Characteristics of the first longitudinal-fourth bending mode linear ultrasonic motors. *Jpn. J. Appl. Phys*., 41: 7139–7143, 2002.

[8] T. Bein, E. J. Breitbach and K. Uchino, A linear ultrasonic motor using the first longitudinal and forth bending mode, *Smart Mater. Struct.* 6, 619–627, 1997.

[9] S. G. Kelly, *Mechanical Vibrations: Theory and Applications*, CENGAGE Learning, USA, 2012.

[10] M. I. Frecker, Recent Advances in Optimisation of Smart Structures and Actuators, *Journal of Intelligent Material Systems and Structures*, Vol. 14—April/May 2003.

[11] P. Ghisbain, Application of Gradient-based Algorithm to Structural Optimization, Master of Science in Civil and Environmental Engineering Thesis, p.17, MIT, Feb. 2009.

[12] K. Uchino, *Piezoelectric ceramics*, Handbook of Advanced Ceramics, S. Sōmiya et al. (Eds), Elsevier, 2003.

[13] UCL Department of Phonetics and Languistics, Introduction to Computer Programming with Matlab, Available at: http://www.phon.ucl.ac.uk/courses/spsci/matlab/lect6.html